Investigation of Mechanical Deformation in Rigid Polymers by 2D Solid-State NMR Imaging

B. Traub, S. Hafner, U. Wiesner, and H. W. Spiess*

MPI für Polymerforschung, Postfach 3148, D-55021 Mainz, Federal Republic of Germany

Received June 29, 1998

ABSTRACT: The use of two-dimensional solid-state NMR imaging for probing variations in the local molecular mobility in cold-drawn rigid polymers is shown. A magic-echo-based 2D solid-state NMR imaging sequence is used that has been supplemented by a T_{2e} relaxation−filter sequence for probing mobility contrast. It is applied for the investigation of polycarbonate samples that have been drawn under different conditions. Characteristic regions of chain immobilization caused by the mechanical treatment are mapped by NMR parameter images, and the results are compared with polarization microscopy images.

Introduction

Failure of polymer materials often results from a nonuniform spatial distribution of the underlying microscopic properties.[1] Such (mostly undesired) spatial variations can be caused by processing conditions or by a later treatment of the material. There is a strong need for techniques by which the macroscopic distribution of molecular parameters can be monitored. The understanding of this distribution as a function of the conditioning of the sample then allows a better control of the resulting macroscopic properties and thus the improvement of the material.

A powerful technique for the characterization of materials is solid-state NMR spectroscopy,[2−5] which provides rich information on structure and dynamics in polymers on various length and time scales, respectively.[4] By combining it with NMR imaging techniques, this information is accessible also spatially resolved. Thus, the macroscopic variation of a given microscopic or mesoscopic property can be investigated nondestructively and, when desired, even in situ.[6]

The high potential of NMR imaging with respect to the characterization of materials has been recognized relatively early, and numerous applications have been shown already. This includes the ingress of liquids in solids[7−9] and the investigation of processes such as the polymerization of polymers,[10] the vulcanization of rubbers,[11] or the swelling of polymer networks.[12] Also the macroscopic spatial distribution of microscopic material properties has been imaged. Examples are images of the cross-link density,[11,12] the orientation in polymers,[13] aging effects,[14] and the immobilization of polymer chains by mechanical deformation.[15] Such macroscopic changes in the material properties usually are not related to significant changes in the material density of the sample. A simple mapping of the spin density therefore is not sufficient, and NMR spectroscopic parameters which are sensitive to the investigated material property have to be incorporated in the imaging experiment. Various relaxation processes such as T_1, T_{1D}, $T_{1\rho}$, T_2, and T_{2e} relaxation have been exploited in NMR imaging experiments so far. The $T_{1\rho}$ relaxation time and the effective transverse relaxation time T_{2e} were found to be particularly sensitive parameters for the molecular dynamics in rigid polymers.[16]

The application of NMR imaging, however, was for a long time restricted to nonrigid solids in which the dominating line-broadening mechanism is partially averaged by thermal motion. Most of the examples discussed above belong to this class. In these cases, the routine imaging techniques used for medical diagnosis can be applied with only minor modifications. In rigid solids, however, this thermal averaging is not efficient, resulting in a large proton line width on the order of tens of kilohertz and a failure of conventional NMR imaging techniques.

To overcome this limitation, considerable efforts in developing suitable techniques have been undertaken the past few years. The proposed techniques are based either on the excessively strong field gradients in the fringe field of a superconducting magnet[17] or on the application of sophisticated line-narrowing techniques during the imaging procedure. ^{1}H solid-state imaging with MAS line narrowing,[18] Lee−Goldburg line-narrowing,[19] multiple-pulse line-narrowing,[16,20−22] constant-time phase-encoding,[23−26] and combinations of these techniques are presently in use. In the following, we will apply a combination of the latter two approaches which is based on the so-called magic echo.[27] This technique has proven to be particularly suitable for the application to polymer materials, since NMR spectroscopic techniques can conveniently be included in the experiment.

Experimental Section

Method. The basic idea behind NMR imaging is the application of magnetic field gradients which render the precession frequency of the spins spatially dependent. Figure 1 shows the radio frequency−pulse (upper line) and gradient timing scheme (middle two lines) of the sequence used for the following investigation. Three main parts can be distinguished:

First, for the time t_1, a relaxation-time filter sequence is applied in order to introduce mobility contrast. It consists of a multiple solid-echo train[28,29] and reduces the dipolar interaction such that the magnetization decays with the relaxation time T_{2e} instead of the conventional transverse relaxation time T_2. Incrementing the time t_1 for successive acquisitions, the relaxation curve is acquired and the corresponding relaxation time can be evaluated. The relaxation time T_{2e} was used for the following experiments since it is found to be very sensitive to the molecular dynamics in polymers, in particular to slow thermal motions of up to about 10^4 Hz.

10.1021/ma981008k CCC: $15.00
Published on Web 11/06/1998

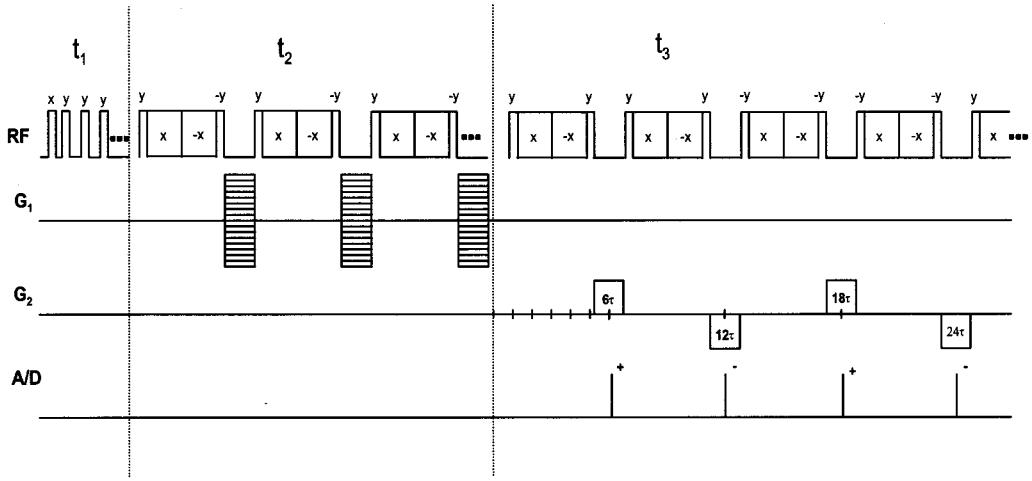

Figure 1. Parameter-selective 2D-FT magic-echo imaging sequence used in the experiments. It consists of a T_{2e}-relaxation-time filter for mobility contrast (time t_1), a multiple-magic-echo phase-encoding imaging part (time t_2), and data acquisition during a multiple-magic-echo imaging sequence (time t_3).

The filter is followed by the two imaging parts during which a series of magic sandwiches is applied. The magic sandwich pulse sequence consists of a long radio frequency $\pm x$ pulse sandwiched between two 90° $\pm y$ pulses. A detailed description of this sequence and its properties can be found in refs 30−32. It is designed such that it reverses the dipolar interaction. Coherences which have been dephased by the dipolar interaction during the free evolution periods of the sequence thus refocus again and form the so-called magic echo. Sampling only the echo maxima of such a pulse train results in a spectrum from which the dipolar interaction has been removed. The gradients therefore have to deal only with relatively narrow lines from which the main line-broadening has been eliminated. They are introduced now in the form of short gradient pulses during the free-evolution periods between the magic sandwiches.

During the period t_2, the spatial encoding in the y direction is achieved by so-called phase-encoding. That is, the y-gradient strength is incremented, and the signal is acquired in a series of experiments as a function of this incrementation. In the t_3 period the signal is finally read pointwise during the free-evolution period of the magic-echo train (see lowest line in Figure 1, where the vertical lines indicate the timing of the acquisition). Note, that some of the phases of the 90° pulses in the magic-sandwich train are different from those used in the t_2 period. This is to eliminate the chemical-shift interaction which otherwise would affect the resolution in this dimension. During the acquisition of the signal, x-gradient pulses are applied for the spatial encoding in the x-direction (frequency encoding). The whole sequence thus is three-dimensional, with two spatial dimensions and one dimension for introducing the imaging contrast (the relaxation time filter).

Samples. All studies were performed on bisphenole-A-polycarbonate samples (PC, Makrolon 2800). The samples for the imaging experiments were prepared by cold-drawing at room temperature to various maximum elongations with a stretching velocity of 0.5 mm/s. Under these conditions the yield point occurred at a stress of approximately 58 MPa and a strain of 6.5%.

Figure 2 shows the drawing scheme and the dimensions of the pieces of sample that have been cut from the drawn PC stripes. Three different geometries have been generated for the imaging experiments. In the first sample, a necking region was produced by drawing the sample up to an elongation of $\lambda = 1.7$. A second sample was prepared by drawing to an elongation of $\lambda = 2.7$. The drawing was stopped shortly before the sample would break in two separate pieces. For the third sample, two crossing shear bands were generated by scratching the specimen on the surface in order to localize and induce the shear zones. Shear bands can be understood as strongly

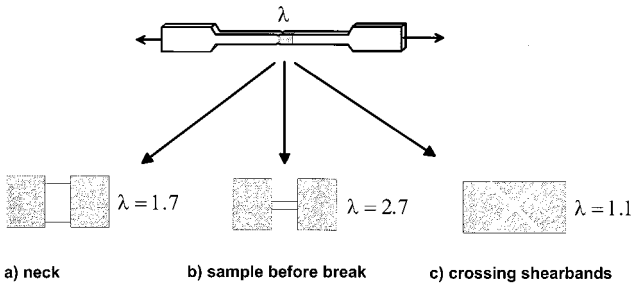

Figure 2. Geometry used for the drawing of the polycarbonate samples. For the imaging experiments, three different kind of deformations have been created: (a) necking region; (b) sample immediately before break; (c) crossed shear bands.

localized inhomogeneities of the plastic deformation. Usually such shear bands form under an angle of 30−45° to the drawing direction. The scratch does not significantly change the measured value of the yield stress. The maximum elongation was $\lambda = 1.1$ in this case.

As reported elsewhere[35] the drawing mainly influences the intermolecular interactions as a result of a change in the packing of the chains. That is, the distribution of the free volume is affected, and a partial orientation of the polymer chains takes place. Also the small amplitude motions of the phenylene rings are influenced by the cold-drawing, thus changing the T_{2e} relaxation rate.

NMR Experiments. The NMR imaging experiments have been performed on a Bruker DSX-300 NMR spectrometer equipped with imaging facilities. The static B_0 field of 7.05 T corresponds to a ^{1}H resonance frequency of 300.23 MHz. A modified static Bruker probe head has been used with a 8 mm solenoid coil. The 90° pulse length was set to 2.5 μs, which corresponds to a B_1 field strength of 100 kHz. Since very fast gradient switching is required, a home-built gradient system has been used which was specifically designed for short gradient rise times.[33] The gradient coils for the x, y, z gradients have a diameter of 25 mm and are optimized for low inductance. They allow a switching time of less than 1 μs so that the gradients can conveniently be switched within the free-evolution periods of the magic-echo pulse train.

The sequence depicted in Figure 1 is applied to polycarbonate samples that have been drawn before the imaging experiment under the different conditions described above. Since polycarbonate is transparent, it allows the application of polarization microscopy for comparison to the NMR imaging results. The experimental parameters for the 2D NMR imaging experiments have been set as follows: The field of view in the images is 12.8 mm × 6.4 mm, and 128 pixels have been acquired in the frequency-encoding and 64 in the phase-

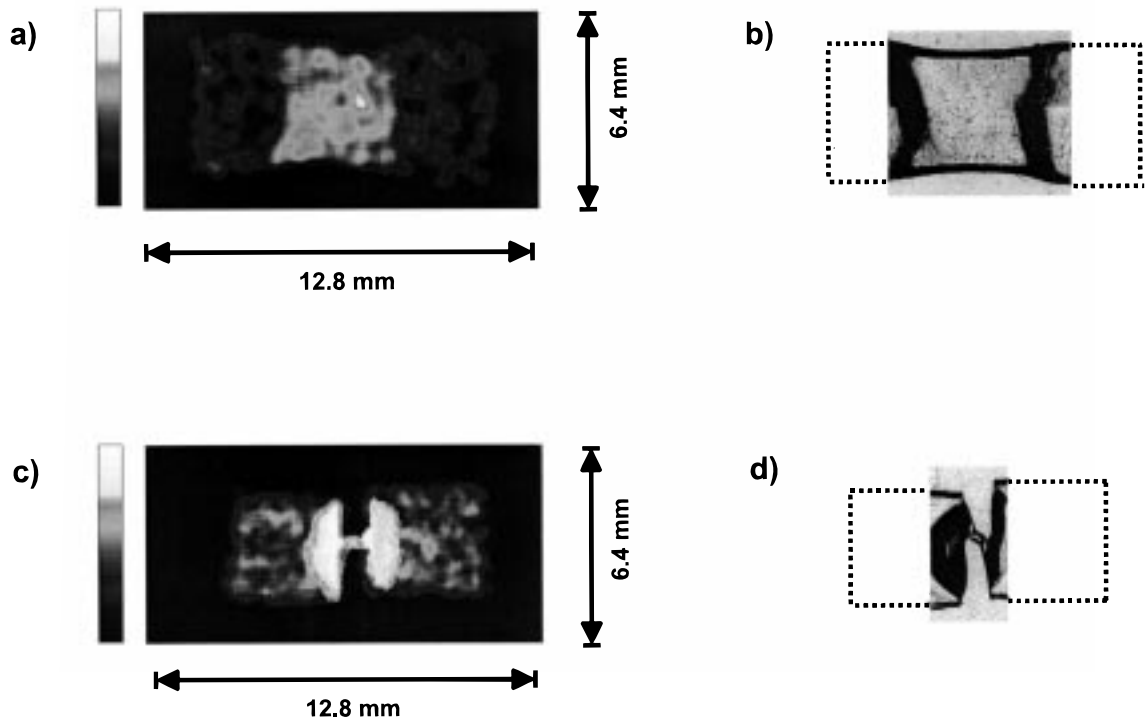

Figure 3. (a) T_{2e}-relaxation-rate image of a piece of drawn polycarbonate showing the necking region at $\lambda = 1.7$. (b) Photograph under polarized light of part of the sample (the shape of the full piece is indicated by the dotted lines). (c) T_{2e}-relaxation-rate image of a piece of drawn polycarbonate showing the region where the break occurs at $\lambda = 2.7$. (d) Photograph under polarized light of the sample corresponding to part c.

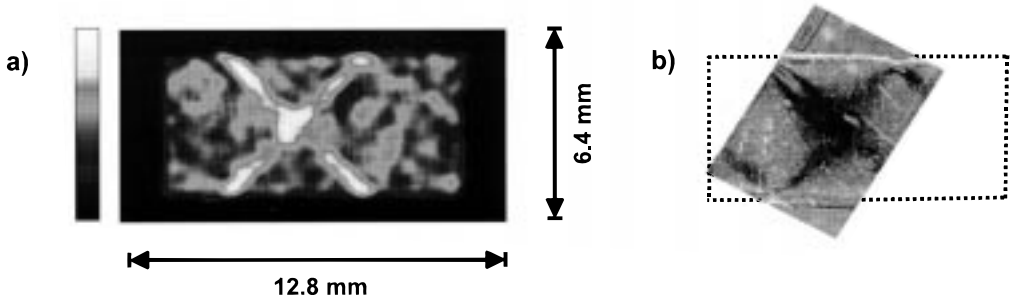

Figure 4. (a) T_{2e}-relaxation-rate image of a piece of polycarbonate in which two crossing shear bands have been generated in comparison with (b) the polarization-microscopy image.

encoding dimensions. This corresponds to an isotropic pixel resolution of 100 μm. The number of echoes during the phase-encoding period was set to 175. In the directly detected t_3-dimension 128 magic echoes have been generated. The cycle time of the magic-echo train was 60 μs for both, the phase-encoding and the frequency-encoding parts. A maximum phase-encoding gradient of 210 mT/m and a frequency-encoding gradient of 46 mT/m have been used. The number of solid echoes in the T_{2e} filter sequence was incremented from 1 to 32, resulting in 32 differently T_{2e}-weighted images. The time between the solid echoes was 18 μs. With a repetition time of 3 s and an accumulation of 8 scans for signal-to-noise improvement, the total time for the experiment was 20 h.

For the evaluation of the relaxation data series, the T_{2e} decay for each spatial coordinate was fitted after normalizing to 100% with the exponential function

$$S(r,t) = A(r) + B(r)\exp(-t/T_{2e}(r))$$

where $B(r)$ denotes the local amplitude of the exponential decay, which is characterized by the local relaxation time $T_{2e}(r)$. The constant $A(r)$ accounts for a constant signal offset which, however, did not appear in our experiments; i.e., $A(r) = 0$. Two parameter maps of the sample are obtained by the fitting procedure. One represents the spin density $B(r)$, while the other gives the effective transverse relaxation rate $1/T_{2e}(r)$. The average error of the fitted values is less than 8%.

The T_{2e} decay in polycarbonate is caused by two components: the phenylene rings and the methyl groups, resulting in a biexponential T_{2e} decay.[34,35] The short-time behavior caused by the phenylene units reflects the intermolecular interactions, whereas the long-time behavior is determined by the methyl groups thus being a probe for intramolecular interactions.[34] The decay rates of the two components, however, differ by less than 1 order of magnitude. For this reason and to ensure the stability of the fitting procedures for all pixels of the image, a monoexponential fit was used in the present investigation.

Results and Discussion

The 2D NMR images of the differently treated polycarbonate samples are shown together with polarization microscopy images in Figures 3 and 4. Apart from some changes of the original shape of the sample due to the drawing, no indications of spatial inhomogeneities are found in the spin density images (data not shown). It is well-known that drawing of such samples is not

accompanied by significant changes in the local material density.[1]

As discussed in previous work,[16,35] the mechanical treatment is revealed in the $1/T_{2e}$ map, which reflects changes in the molecular dynamics. Figure 3a shows the $1/T_{2e}$ map of the sample drawn to $\lambda = 1.7$ in which a necking region has been created (note that the rate $1/T_{2e}$ is displayed in all images). The T_{2e} relaxation rate close to the right and left borders of the sample, that is, in the unaffected parts, is $1/T_{2e} = 11.8 \times 10^3$ s^{-1}. For the necking region in the center it increases to $1/T_{2e} = 20.5 \times 10^3$ s^{-1}. These values are in agreement with a previous one-dimensional investigation.[34] As already discussed there, the change in $1/T_{2e}$ corresponds to a temperature shift of around 85 ± 20 K between the affected and unaffected parts of the sample, and the immobilization detected by T_{2e} reflects predominantly a change in the small-amplitude phenylene motion. In constrast to this, the change in the overall density between the affected and unaffected parts corresponds to a temperature shift of about 10 K only.

For comparison, a photograph of the investigated sample has been taken under a polarizing light microscope (see Figure 3b). The affected regions of the sample are also distinguished in the polarization microscopy image, thus confirming the result of the NMR imaging experiment. While the NMR imaging experiment reflects the dynamics, the polarization microscopy image contains information on the stress distribution. From the latter the local stress appears to be strongest at the borders of the immobilized region, while the transmission of light is essentially unaffected in the center parts.

As a second example, Figure 3c shows the $1/T_{2e}$ image of a cold-drawn polycarbonate sample which was drawn up to a maximum elongation of $\lambda = 2.7$. Before the total failure of the material occurred, a sort of second neck grew within the original necking region and became thinner with increasing elongation until the sample finally broke in two parts. The actual geometry is determined by microscopic defects that are randomly distributed in the material and that lead to a localization at one point where the sample starts to break. For the sample used in the imaging experiment, the drawing was terminated just a moment before total failure.

Figure 3d shows the photograph of the affected polymer region under polarized light. Around the region of the thin material bridge between the two parts, dark regions are shown which are shaped in the form of a half-circle. These regions represent frozen stress. The 2D NMR image (Figure 3c) reveals that these regions correspond also to low molecular mobility. That is, an increase of the T_{2e} relaxation rate is found there. The $1/T_{2e}$ value in these regions is $1/T_{2e} = 32.3 \times 10^3$ s^{-1}, while for the outer parts of the sample one finds 20.8×10^3 s^{-1}. The latter corresponds to the value of the necking region found above for the first sample (see Figure 3a) and serves as a further check for the consistency of the experiments since the outer parts of the sample in Figure 3c also represent this necking region. The former shows that the immobilization in the regions close to the thin material bridge is substantially higher.

As an example for the investigation of a related deformation mechanism we have already studied isolated shear bands using NMR imaging.[16,35] Here, we want to extend this study to the case of two shear bands which cross each other. Figure 4a shows a $1/T_{2e}$ image of a sample in which two crossing shear bands have been generated by systematically scratching the surface. When preparing the sample carefully, the occurrence of crazes can be ruled out. While the spin density image (not shown) again does not reveal the affected regions, the crossed shear bands are clearly visible in the $1/T_{2e}$ map. The average relaxation rate inside the shear bands is $1/T_{2e} = 13.2 \times 10^3$ s^{-1}. Though clearly distinguishable from the unaffected part which has a value of $1/T_{2e} = 11.5 \times 10^3$ s^{-1}, the immobilization is less pronounced than that found in Figure 3a for the necking region (note that in the case of the shear bands, a deformation of only $\lambda = 1.1$ was applied). At the crossing point of the two shear bands the T_{2e} relaxation rate is $1/T_{2e} = 13.7 \times 10^3$ s^{-1}, that is, almost the same as in each one alone. This means that, as far as the molecular dynamics is concerned, the effects of the two shear bands do not interfere with each other.

For comparison, the photograph under polarized light is presented in Figure 4b. The crossed shear bands are clearly visible as dark regions. Moreover, further shear bands are visible, which start at the edges of the sample under an angle of 90° to the center shear bands (see Figure 4b). Closer inspection of the NMR image in Figure 4a also reveals indications of these bands which might have been misinterpreted at first sight as noise.

Conclusions

Solid-state NMR imaging has developed to a point where it becomes useful for the investigation of spatially resolved structural and dynamical heterogeneities in rigid polymers. We have shown that phenomena related to the failure of rigid polymers under large mechanical stresses can be investigated by this technique. In this way, correlations between microscopic parameters, like the relaxation rate T_{2e}, and macroscopic features such as shear bands, can be set up. The results have been compared to polarization microscopy data, which was possible because the investigated polycarbonate samples are transparent. Such a limitation, of course, does not apply to the NMR imaging technique which therefore is more generally applicable. Whenever possible, both techniques should be combined since they provide supplementary information on the sample.

As a solid-state NMR imaging method, magic-echo-based techniques have been used and have proven to provide satisfactory resolution in a comparatively easy way. In particular, the phase-encoding variant in its simplest form can be applied on any spectrometer with imaging equipment since it does not require any specific hardware. But also when the frequency-encoding variant is used as in the presented experiments, the magic-echo pulse sequence is much more forgiving with respect to misadjustments and allows longer free-evolution periods for the spatial encoding than other multiple-pulse techniques.

When NMR imaging is compared with other microscopy techniques, one drawback is the lower resolution, even under optimum conditions. There are many applications, however, for which the presently achievable resolution of solid-state NMR imaging of the order of 100 μm is sufficient and the possibility to incorporate the full NMR spectroscopic information is an invaluable advantage. Rather than optimizing the resolution to the ultimately possible limit of around $(10\ \mu\text{m})^3$, in the present work, we thus concentrated on introducing

NMR spectroscopic parameters to provide information that is not accessible by other techniques. Microscopic properties as derived from NMR spectroscopy or relaxation measurements can be correlated with the macroscopic structures that are accessible by NMR imaging. As an example we have investigated polycarbonate samples which have been drawn under various conditions and could locate the regions of reduced molecular mobility.

Acknowledgment. The authors would like to thank Dr. A. Karbach, Bayer AG, Leverkusen, for providing the polycarbonate, Dr. T. Pakula for assistance with the mechanical experiments as well as for fruitful discussions, and J. Vennemann for the drawing of the samples.

References and Notes

(1) Haward, R. N. *The Physics of Glassy Polymers*; Applied Science Publishers Ltd.: London, 1973.
(2) Ibett, R. N., Ed. *NMR Spectroscopy of Polymers*; Blackie Academic & Professional: London, 1993.
(3) McBrierty, V. J.; Packer, K. J. *NMR in Solid Polymers*; Cambridge University Press: Cambridge, U.K., 1993.
(4) Schmidt-Rohr, K.; Spiess, H. W. *Multidimensional Solid State NMR and Polymers*; Academic Press: London, 1994.
(5) Mehring, M. *High-Resolution NMR in Solids*; Springer: London, 1983.
(6) Blümich, B., Kuhn, W., Eds. *Magnetic Resonance Microscopy: Methods and Applications in Materials Science, Agriculture and Biomedicine*; VCH: Weinheim, Germany, 1992.
(7) Webb, A. G.; Hall, L. D. *Polymer* **1991**, *32*, 2927.
(8) Mansfield, P.; Bowtell, R.; Blackband, S. *J. Magn. Reson.* **1992**, *99*, 507.
(9) Hafner, S.; Kuhn, W. *Magn. Reson. Imaging* **1994**, *12*, 1075.
(10) Klei, B.; Koenig, J. L. *Acta Polym.* **1997**, *48*, 199.
(11) Fülber, C.; Unseld, K.; Herrmann, V.; Jakob, K. H.; Bluemich, B. *Colloid Polym. Sci.* **1996**, *3*, 191.
(12) Smith, S. R.; Koenig, J. L. *Macromolecules* **1991**, *24*, 3496.
(13) Günther, E.; Blümich, B.; Spiess, H. W. *Macromolecules* **1992**, *25*, 3215.
(14) Barth, P.; Hafner, S.; Kuhn, W. *J. Magn. Reson.* **1994**, *A110*, 198.
(15) Bluemler, P.; Bluemich, B. *Acta Polym.* **1993**, *44*, 125.
(16) Weigand, F.; Hafner, S.; Spiess, H. W. *J. Magn. Reson.* **1996**, *A120*, 201.
(17) Samoilenko, A. A.; Zick, K. *Bruker Rep.* **1990**, *1*, 40.
(18) Scheler, U.; Titman, J. J.; Blümich, B.; Spiess, H. W. *J. Magn. Reson.* **1994**, *A107*, 251.
(19) de Luca, F.; Lugeri, N.; De Simone, B. C.; Maraviglia, B. *Magn. Reson. Imaging* **1992**, *10*, 765.
(20) Cory, D. G.; Miller, J. B.; Turner, R.; Garroway, A. N. *Mol. Phys.* **1990**, *70*, 331.
(21) Matsui, S. *Chem. Phys. Lett.* **1991**, *179*, 187.
(22) Weigand, F.; Blümich, B.; Demco, D. E.; Spiess, H. W. *Solid State NMR* **1995**, *6*, 357.
(23) Hafner, S.; Demco, D. E.; Kimmich, R. *Meas. Sci. Technol.* **1991**, *2*, 882.
(24) Demco, D. E.; Hafner, S.; Kimmich, R. *J. Magn. Reson.* **1992**, *96*, 307.
(25) Hafner, S.; Barth, P.; Kuhn, W. *J. Magn. Reson.* **1994**, *A108*, 21.
(26) Hepp, A.; Miller, J. B. *J. Magn. Reson.* **1994**, *A111*, 62.
(27) Schneider, H.; Schmiedel, H. *Phys. Lett.* **1969**, *30A*, 298.
(28) Ostroff, E. D.; Waugh, J. S. *Phys. Rev. Lett.* **1966**, *16*, 1097.
(29) Mansfield, P.; Ware, D. *Phys. Rev.* **1968**, *168*, 318.
(30) Rhim, W.-K.; Pines, A.; Waugh, J. S. *Phys. Rev. Lett.* **1970**, *25*, 218.
(31) Rhim, W.-K.; Pines, A.; Waugh, J. S. *Phys. Rev. B* **1971**, *3*, 684.
(32) Hafner, S.; Demco, D. E.; Kimmich, R. *Solid State NMR* **1996**, *6*, 275.
(33) Weigand, F.; Blümich, B.; Spiess, H. W. *Solid State NMR* **1994**, *3*, 59.
(34) Weigand, F.; Spiess, H. W. *Macromolecules* **1995**, *28*, 6361.
(35) Weigand, F.; Wiesner, U.; Spiess, H. W. *Adv. Mater.* **1996**, *8*, 481.
(36) Gedde, U. W. *Polymer Physics*; Chapman & Hall: London, 1995.

MA981008K